Effects of radar side-lobes on snow depth retrievals from Operation IceBridge

R. KWOK,[1] C. HAAS[2]

[1]*Jet Propulsion Laboratory, California Institute of Technology, Pasadena, CA, USA*
[2]*York University, Toronto, Ontario, Canada*
Correspondence: R. Kwok <ron.kwok@jpl.nasa.gov>

ABSTRACT. Arctic snow depth data products from four years (2009–12) of Operation IceBridge (OIB) surveys are examined. In our analysis, we found spurious spikes in the snow depth distributions of both the multi-year and seasonal ice covers. These spikes are artifacts that stem from the incorrect identification of side lobes and main lobes of the impulse response of the snow radar as returns from the air–snow interface. The current OIB snow depth retrieval algorithm does not explicitly account for the presence of these side lobes and main lobes. As a result, overall accuracy of snow depth returns and related statistics is negatively affected. Although the range locations of these side lobes are predictable for each radar installation, they vary with individual airborne campaigns. Comparisons with limited in situ snow surveys show significant differences of >20 cm between OIB and in situ snow surveys. These artifacts affect OIB ice thickness estimates because they rely on estimates of sea-ice freeboard, which are calculated as the differences between coincident snow freeboard from lidar elevations and the retrieved snow depth estimates discussed here. Since these products are widely distributed to the scientific community, our results suggest that earlier geophysical studies based on these products may need to be re-examined.

KEYWORDS: remote sensing, sea ice, snow, snow/ice surface processes

1. INTRODUCTION

NASA's Operation IceBridge (OIB) (Koenig and others, 2010) was implemented as an airborne remote-sensing program to extend the time series of lidar altimetry over sea ice and ice sheets through the gap between the end of ICESat (Ice, Cloud and land Elevation Satellite) data collection in 2009 and the launch of ICESat-2 lidar in 2017. Recognizing the importance of snow depth in controlling surface heat balance and for the determination of snow loading in altimetric ice thickness retrievals, the OIB airborne instrument suite includes an ultra-wideband frequency-modulated continuous-wave (FMCW) radar for measuring snow depth. Since 2009, OIB has conducted annual spring surveys to acquire data over both the Arctic and Antarctic sea-ice covers. The long OIB flight tracks, some exceeding 3000 km in length, have been designed to sample a diverse range of ice and snow conditions. Early assessments of some of these datasets of the Arctic can be found in Kurtz and Farrell (2011), Kwok and others (2011) and Farrell and others (2012).

From the datasets acquired by the suite of airborne instruments, the OIB project provides operational data products that contain retrievals of sea-ice freeboard, snow depth and thickness using algorithms described by Kurtz and others (2013). These products are available at the US National Snow and Ice Data Center (NSIDC) and have been used in a number of studies including cross comparisons with satellite and aircraft retrievals (e.g. Brucker and Markus, 2013; Laxon and others, 2013), the documentation of recent ice conditions (e.g. Richter-Menge and Farrell, 2013), the initialization of seasonal forecasts (e.g. Lindsay and others, 2012) and the estimation of decadal trends in Arctic snow depth (Webster and others, 2014). In this paper, we offer insights into artifacts that were not accounted for in the OIB snow depth retrievals. The term artifacts refers to retrieval errors due to side lobes in the system impulse response. These artifacts affect the accuracy of the snow depth products and suggest that geophysical results from earlier studies (e.g. those cited earlier in this paragraph) may need to be re-examined.

At the time of writing, four years of these retrievals from the Arctic OIB campaigns (2009–12) are available and the expected quality of these retrievals is summarized by Kurtz and others (2013). However, the overall quality of these products is difficult to assess due to a lack of sufficient coincident in situ validation data that cover a range of snow and ice conditions. In a recent examination of snow depth retrievals using OIB snow radar data over the Weddell and Bellingshausen Seas, Kwok and Maksym (2014) reported that side lobes of the radar system response could introduce artifacts when the strength and location of these side lobes are not explicitly addressed. In a bandwidth-limited radar system, side lobes occur before and after the main lobe in the return, and the leading side lobes from the stronger scattering snow–ice interfaces could be misidentified as returns from the weaker air–snow interfaces in the retrieval processes. Kwok and Maksym (2014) also noted that these artifacts should be visible in large-scale snow depth distributions since the range locations of the side lobes (relative to the main lobe; see description in Section 3) in the radar return are predictable. If these artifacts were present in snow depth retrievals, the sea-ice thickness estimates in the OIB products would also be affected because they depend on ice freeboard retrievals, which are computed as the difference between the snow freeboard from the Airborne

https://doi.org/10.3189/2015JoG14J229 Published online by Cambridge University Press

Topographic Mapper (ATM) lidar elevations and the OIB snow depth estimates.

The subject of this paper is an examination of the phenomenology of side lobes and main lobes in the four years (2009–12) of Arctic OIB snow radar data and their impact on the snow depth product and associated errors. The intent here is to identify and highlight issues in the current OIB snow depth data product available at the NSIDC, and to note that if specific system response characteristics (i.e. range-varying impulse response for each OIB campaign) were not identified and accounted for, the side lobes would affect the results of snow depth statistics and their use in geophysical investigations. We suggest that our results should be considered in future improvements of the processing algorithms and revisions of the OIB data product. The paper is organized as follows. Section 2 describes the datasets used in the following analyses. Section 3 provides a brief description of the source of the side lobes, shows the spikes in the overall snow depth distributions in the four years of OIB data products, and discusses the effects of system side-lobes in the detection of air–snow interfaces. Section 4 assesses the Arctic snow depth distribution produced in the OIB products and compares the OIB snow depths with in situ data from ground surveys (Willat and Haas, 2011; Webster and others, 2014). Summary remarks and conclusions are provided in the last section.

2. DATA DESCRIPTION

We use three OIB data products from the Arctic campaigns in 2009 through 2012. They include: (1) the Level 1B Geolocated Radar Echo Strength Profiles (RESP) (Leuschen, 2010), which contain the radar echoes from the Center for Remote Sensing of Ice Sheets (CReSIS) ultra-wideband FMCW snow radar over sea ice; (2) the Level 1B ATM Elevation and Return Strength dataset (Krabill, 2013), which contains the ATM spot elevation measurements over sea ice; and (3) the Sea Ice Freeboard, Snow Depth and Thickness (FSDT) dataset (Kurtz and others, 2012), which contains the parameters derived from the combined OIB Snow Radar, Digital Mapping System (DMS), Continuous Airborne Mapping By Optical Translator (CAMBOT) and ATM datasets. The DMS provides high-resolution digital imagery while the CAMBOT provides lower-resolution camera images. The reader is referred to the published literature for more detailed descriptions of the radar (Panzer and others, 2013) and lidar systems (Krabill and others, 2002; Martin and others, 2012). We note that the 2009 and 2010 snow radar data are distributed in individual files, each containing ~4000 radar echoes with a nominal ground separation of ~1 m between echograms. At an altitude of ~500 m, the nominal footprint size of the snow radar is ~6 m and the range resolution is typically ~6 cm but varies with operational bandwidth. To suppress system noise, echograms during and after 2011 are averages of five radar returns (incoherently averaged); this reduces the number of echograms to 1000 per file, spaced every 4 m along the ground track. The standard sea-ice freeboard, snow depth and thickness are provided at a length scale of ~40 m from available along-track measurements. In the OIB snow depth algorithm, the air–snow interface, defined relative to the snow–ice interface, is either the location of the first local maxima in the return or the point of continuous power increase (i.e. a well-defined edge) (Kurtz and others, 2013); their best estimate of the error in snow depth retrieval is ~6 cm without considering the impact of side lobes (discussed here).

In situ snow depth measurements are from the CryoVEx 2011 CryoSat Validation Experiment coordinated by the European Space Agency (ESA) (Willat and Haas, 2011). On 15 April 2011, the IceBridge P-3 overflew CryoVex's south site located on multi-year (MY) pack ice ~120 km north of Ellesmere Island, Canada. Here we use 99 snow depth measurements obtained with a metal snow probe along a 430 m long profile (Willat and Haas, 2011). For guiding aircraft overflights over the snow profile, GPS buoys, corner reflectors and visible markers (bin bags and tarpaulins) were deployed as navigation aids and to provide position information for surveys at different times over the drifting pack ice.

3. DATA ANALYSIS

This section is divided into three parts. We first show that recurring spikes occur in overall snow depth distributions computed from the OIB products (2009–12). Second, we illustrate the expected occurrence of system main- and side-lobes using returns from a flat surface, and discuss how their strength and peakiness impact the snow depth retrieval algorithm. Third, we show the correspondence between the main-/side-lobe locations and the spikes in the snow depth distributions in four years of OIB retrievals.

3.1. Snow depth distributions (2009–2012)

Figure 1 shows the snow depth distributions along the OIB tracks in three different MY sea-ice regimes (color coded: low (<0.3), moderate (0.3–0.7) and high MY (>0.7) fractions). In all four years, as expected, higher mean snow depth is found in regions with higher MY sea-ice coverage. Closer examination, however, shows spikes in the snow depth distributions that are most apparent in 2011 and 2012 but less so in 2010 and 2009 (discussed later). In 2011, distinct spikes in the distributions are seen at close to the same snow depth (~24 cm) at both moderate and high MY ice fractions. Also of note is the surprisingly large sample population below the expected resolution of the radar: the radar system is not expected to resolve separations of <6–7 cm between the air–snow and snow–ice interfaces (Kwok and others, 2011). In 2012, there are spikes at a snow depth of ~12 cm present in the distributions with low, moderate and high MY coverage. Clearly, the near alignment of these prominent spikes in the snow depth distributions at different MY fractions suggests artifacts in the retrievals (due to system side-lobes) that were discussed by Kwok and Maksym (2014).

We also note that spikes at small snow depths could also result from thin snow on refrozen leads and interspersed thinner first-year ice. However, the occurrence of significant areal fractions of such ice in the MY ice regimes considered here is very unlikely.

3.2. Main lobes and side lobes in the system impulse response

In brief, we describe the source of the main lobe and side lobes in the processed FMCW radar returns. A FMCW radar transmits a linear frequency-modulated signal with a given bandwidth (BW), and receives a delayed and attenuated copy of the scattered radar wave from a target (Fig. 2a). The received signal and a copy of the transmitted signal are then multiplied together, in a process known as deramping (to

https://doi.org/10.3189/2015JoG14J229 Published online by Cambridge University Press

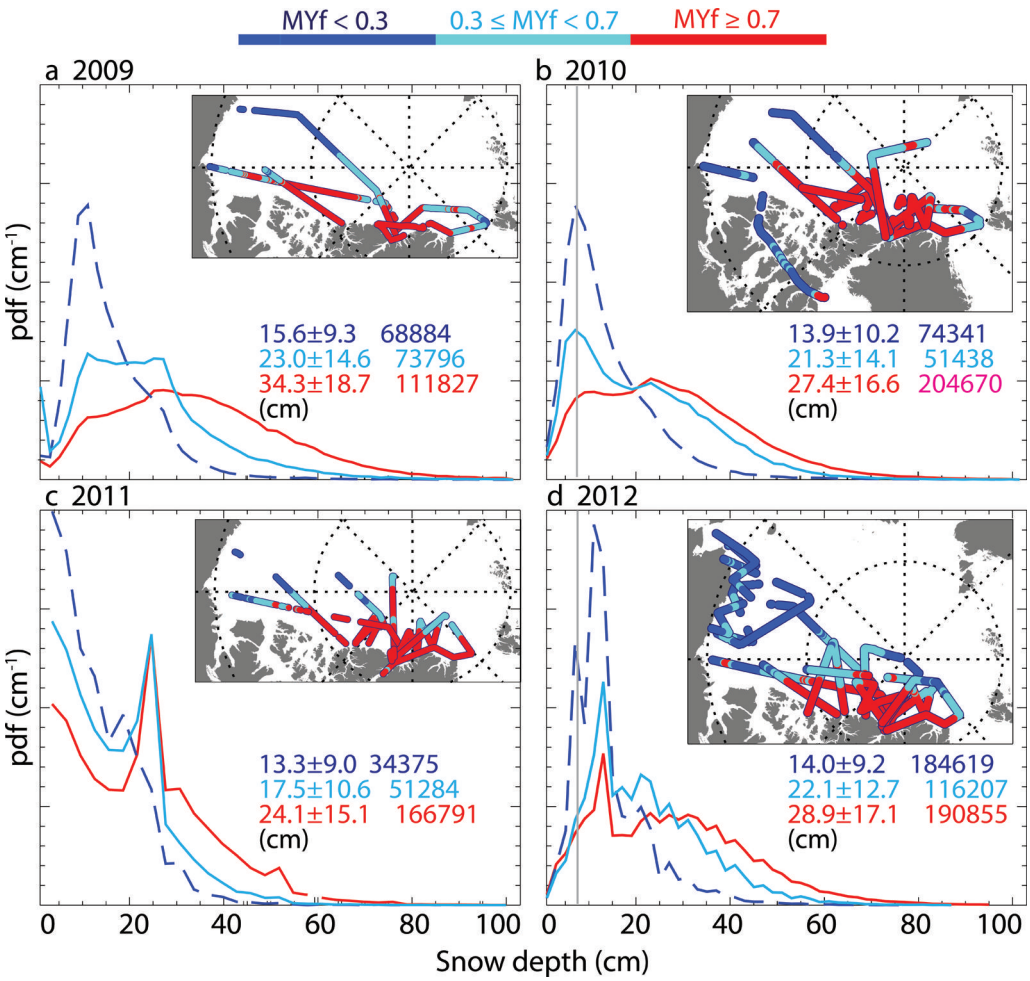

Fig. 1. Snow depth distributions from different MY sea-ice regimes in (a) 2009, (b) 2010, (c) 2011 and (d) 2012. MYf is multi-year sea-ice fraction; pdf is probability density function. Insets show the MY sea-ice fraction along OIB ground tracks. Numerical values show mean and standard deviation of the distributions and number of samples used to construct the distributions. Vertical lines (gray) in each plot indicate the expected snow depth resolution of the radar of ~6–7 cm.

remove the linear frequency ramp), to produce a difference signal (which contains a beat frequency) that is directly proportional to the two-way time delay to a surface (Fig. 2b). In snow depth retrieval, it is the range or time delay between the air–snow and snow–ice surfaces that is of interest. The frequency analysis of the deramped signal results in a main lobe centered at the beat frequency flanked by side lobes (Fig. 2c). The width of the main lobe (or concomitantly the range resolution of the system) in time is dependent on the bandwidth of the radar, with the range resolution improved with higher bandwidth. But side lobes, which could potentially confound the detection of the weaker of the two interfaces, are characteristics inherent in the finite time duration (T) of the sampled signal. There are approaches to suppress side lobes, and the reader is referred to Panzer and others (2013) for a more detailed description of the OIB snow radar and the processing procedures used to produce the return profiles.

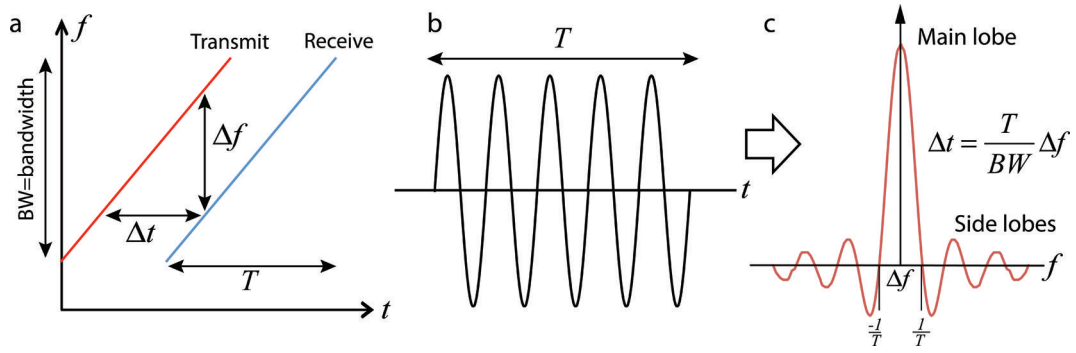

Fig. 2. Operating principle of FMCW radars. (a) Frequency-modulated transmitted and received signals with bandwidth (BW). (b) Deramped signal containing beat frequency (Δf). (c) Analysis of the frequency of the deramped signal to obtain Δfresults in a main lobe with associated side lobes due to the finite time duration (T) of the sampled signal; the two-way time delay (Δt) is then calculated using Δf.

https://doi.org/10.3189/2015JoG14J229 Published online by Cambridge University Press

Figure 3a shows the radar return from relatively flat surfaces of thin ice or open water (near-specular) in the 2011 Arctic dataset, similar to data shown by Kwok and Maksym (2014) for Antarctic sea ice. The *x*-axis corresponds to the radar range in snow, with the radar wave traveling from the radar at the right to the snow–ice interface at the left. Travel times have been converted into range-in-snow by taking into account the reduced propagation speed in snow. A peak in the return with an associated main lobe and side lobes typically characterizes the radar echo from a flat surface (e.g. the snow–ice interface). As discussed above, the finite width (w) of the main lobe at the half-power point (i.e. 3 dB below the peak) defines the range resolution of the radar. The side lobes associated with the main lobes have varying strengths; they are artifacts due to the limited temporal duration of the radar returns and thus are characteristic of the measurement system. Note that these side lobes occur before and after the main lobe. When these artifacts were unaccounted for, the side lobes from the stronger scattering snow–ice surface can be misidentified as returns from the weaker air–snow surface in retrieval procedures used to locate the air–snow and snow–ice interfaces.

We follow the definitions employed by Kwok and Maksym (2014) to examine and visualize the average strength and structure of system side-lobes in the snow radar datasets. We define the maximum value in a sampled snow radar profile, $s(i)$, to be $s_{\mathrm{peak}} = \arg\max s(i)$ (where arg max is the argument of the maximum). The peak signal-to-noise ratio, $\mathrm{PSNR} = s_{\mathrm{peak}}/\overline{n}$, provides a measure of the strength of the peak return relative to the system noise level $\overline{n}$. We compute the $\overline{n}$ noise level using the first 100 samples in each return. With these definitions, we can examine the dependence of the strength of system side-lobes on PSNR in the 2011 RESP data; these are shown in the family of curves (Fig. 3). Each normalized curve (i.e. $\widetilde{s}(i) = s(i)/s_{\mathrm{peak}}$) in Figure 3 is constructed from echograms acquired over snow-covered sea ice averaged over 1 dB intervals of PSNR from all the echo returns in the 2011 campaign (i.e. the entire dataset of $\sim 1.54 \times 10^6$ returns). For example, the first blue line in the plot is the average normalized return for all samples with a PSNR between 10 and 11 dB. The peaks are more evident for the high PSNR curves. There are 32 such curves where the PSNR ranges from 10 (blue) to 41 dB (red).

Figure 3 shows that the highest side lobe in the 2011 dataset is located at ~24 cm. This side lobe presents itself as a well-defined local maximum and could be misidentified as returns from the air–snow interface. Furthermore, with this highest radar side-lobe at ~16 dB below the main peak, unambiguous detection of air–snow interfaces at radar ranges that are close to the location of these side lobes would require special attention to avoid erroneous snow depths (artifacts) in the retrieval process. Depending also on the sensitivity of the retrieval procedures, smaller side lobes away from the main lobe of the return could be problematic as well. In general, the potential impact of side lobes on retrievals is dependent on the relative strength of the side lobe and air–snow interface at the range location of the air–snow interface.

Side lobes have three notable characteristics (Fig. 3): (1) they are stronger and more easily misidentified as air–snow returns when the returns from the snow–ice interface are strong; (2) their levels (relative to the main lobe) generally decay with distance from the snow–ice return; and (3) in the case of the OIB snow radar, their range locations remain relatively stationary during a given campaign unless changes are made to the radar installation. Further, as can be seen in Section 3.3, the number of side lobes and the steepness of their transitions also vary between campaigns. Side lobes associated with strong snow–ice returns (i.e. high PSNR; red curves) can be mistaken for air–snow returns in the retrieval process. As the PSNR decreases, the side lobes become buried in the noise and become less of an impact on peak detection; however, this is not a desirable scenario as it also reduces the system sensitivity to weaker returns from the air–snow interface. Further, side-lobe levels are typically higher with proximity to the snow–ice peak, although their locations do not vary with signal strength.

Clearly, retrieval errors associated with system side-lobes will bias local snow depth statistics by introducing spurious populations into different parts of the distributions. However, the effects on regional mean snow depth may not be as clear if the accumulated errors in snow depth retrievals add to zero. Accounting for and understanding the effects of the side lobes are thus important in any approach for reliable detection of the location of the air–snow interfaces.

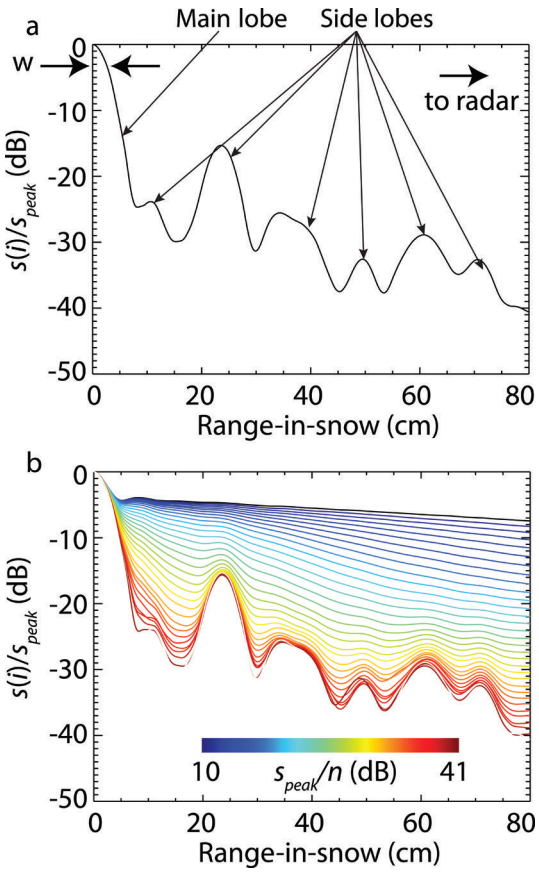

Fig. 3. System main lobes and side lobes in the 2011 Arctic snow radar returns. (a) Snow radar return from a relatively flat surface (only half the return is shown here). w is the half-width of the main lobe. (b) Dependence of strength and location of system side-lobes on signal-to-noise levels. Family of curves shows the averaged normalized returns ($\widetilde{s}(i) = s(i)/s_{\mathrm{peak}}$, where $s_{\mathrm{peak}} = \arg\max s(i)$) at different peak signal-to-noise ratios ($\mathrm{PSNR} = s_{\mathrm{peak}}/\overline{n}$) from all radar profiles. Normalized returns ($\widetilde{s}(i)$) are for every 1 dB increment of PSNR between 10 and 41 dB. All profiles are oversampled by a factor of 16. Range-in-snow is radar range divided by the refractive index of snow (with a bulk density of 320 kg m^{-3}).

https://doi.org/10.3189/2015JoG14J229 Published online by Cambridge University Press

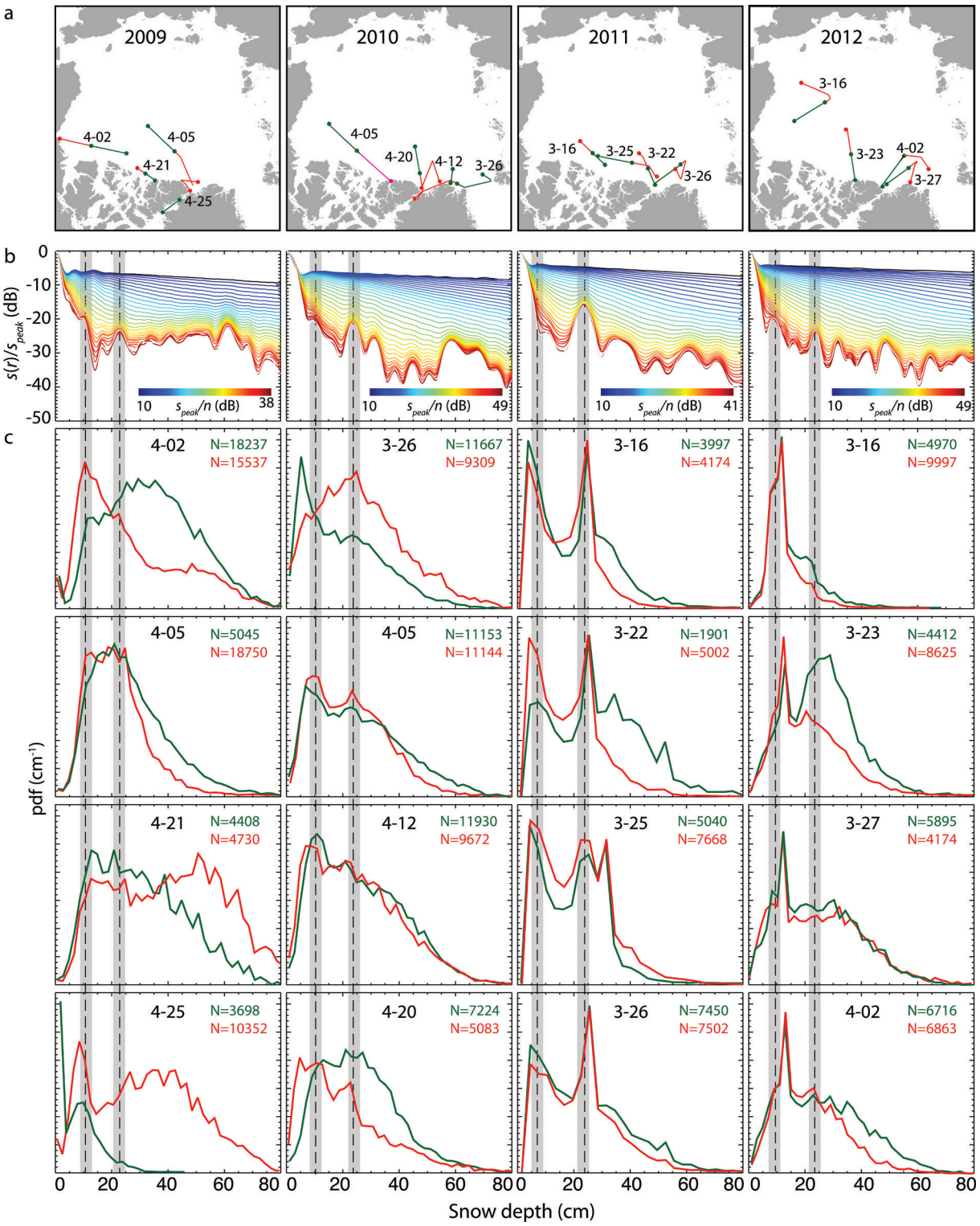

Fig. 4. Effects of side lobes on OIB snow depth distributions from four OIB Arctic deployments (2009–12). (a) Tracks on different dates selected to illustrate effects of side lobes. (b) Same as Figure 3b except for radar installations on 2009, 2010, 2011 and 2012. (c) Snow depth distributions for the tracks/dates shown in (a). Quantities in top right-hand corner of each panel show number of snow depth retrievals (40 m sample^{-1}) in each of the tracks. (Bin size = 3 cm, except for 2012 bin size = 2 cm to resolve narrower spike.) Dashed lines show locations of the peaks of the side lobes.

3.3. Regional snow depth distributions from OIB

Since the locations of side lobes are stationary for a given radar installation, systematic errors in the identification of air–snow returns will appear as anomalous spikes in the derived large-scale snow depth distributions. In Figure 4, we select snow depth distributions from 32 OIB track segments (each 300–500 km in length) from the four years (2009–12) to illustrate the correspondence between spikes in the snow depth distributions and the locations of side lobes.

The expected dependence of the strength of system side-lobes on PSNR for the four years (Fig. 4b) is constructed using the same procedure described above. The side lobe structure (the number, location and sharpness) of each radar installation is different for each year. Even though the

https://doi.org/10.3189/2015JoG14J229 Published online by Cambridge University Press

general radar parameters remain unchanged, any modification to the snow radar hardware (e.g. antennas, cables, electronics, etc.) with every installation on the aircraft platform alters the structure of the side lobes (Fig. 4b). For instance, there are more side lobes in 2012, and with apparently steeper sides, than in 2011. The plots also show the lowest range of PSNRs in 2009 (10–38 dB) with the first deployment of the radar. By far the strongest side lobe at ~16 dB below the main peak is found in the 2011 radar installation; in other years they are all below –20 dB.

Figure 4c shows the snow depth distributions from the 32 segments. We discuss spikes at two locations (dashed lines in Fig. 4) that stand out in the 2011 snow depth distributions. The set of spikes at a snow depth of ~24 cm, aligned with one of the side lobes of the radar system, is present in all eight segments. We attribute the offsets of several centimeters between side lobes and spikes to binning (bin size = 3 cm) and quantization effects due to sampling of the snow radar profiles. Since, as mentioned earier, the current OIB algorithm (Kurtz and others, 2013) uses either the local maxima or leading edge to locate the air–snow interface, the offset of several centimeters toward the leading edge of the side lobes in certain instances is expected. There is no identifiable side lobe associated with the second set of spikes at ~7 cm, but they appear to be tied to the steep rise to the peak of the main lobe. In this case, these spikes may be associated with the leading edge of the main lobe. Since both sets of spikes appear at consistent snow depth locations over a fairly broad geographic region, we presume them to be artifacts of the retrieval process. Over the generally thicker snow cover at the end of winter the spikes at a thinner snow depth lead to an underestimation of the overall mean snow depth when retrieved values from OIB surveys are used. The spikes at ~24 cm affect the segment mean snow depth differently depending on how close they are to the mean regional snow depth, which differs over seasonal or MY sea ice.

The most prominent spikes in the 2012 distributions are located at a snow depth of ~12 cm. Similarly, this set of spikes (associated with the leading edge of side lobe at ~10 cm) is found in different segments across the Arctic: in the seasonal ice (16 March), in the thicker MY ice (23 March) in the central Arctic, and north of the Greenland coast (27 March, 2 April). The location of this spike is especially problematic in seasonal ice segments since these artifacts in retrieval may dominate the sample population and impact the calculated mean snow depth. This spike at the thinner snow depth, however, seems to stand out in the background of the broader snow depth distributions and may be separable from the thicker distribution. The local peaks in the distributions hint at a spike due to a side lobe at ~24 cm, but the level of the expected side lobe is lower and therefore less of an effect (or noticeable) on the retrieval.

In 2010, there are spikes in all eight segments that seem to be associated with the side lobe at ~24 cm. The spikes in both 2010 and 2009 (discussed next) are not as sharp as, and are broader than, those in 2011 and 2012, likely because of noisier radar data (mentioned earlier) used in the retrieval process. The spikes at ~10 cm, likely associated with the leading edge of the main lobe, are present (visible) in only five of the eight segments.

As in 2010, the 2009 spikes at ~10 and ~25 cm are there but are not as noticeable. We also note that the level of side lobe at ~24 cm is at –25 dB, and thus may be less of an issue for the detection scheme (Kurtz and others, 2013).

The spikes in the 32 snow depth distributions shown here point to systematic errors in the retrieval of snow depth that are associated with system main- and side-lobes, and indicate that these sources of errors should be considered in the use of these products.

4. COMPARISON OF OIB SNOW DEPTHS WITH THOSE FROM GROUND SURVEYS

Here we compare the OIB snow depth retrievals with ground surveys during the April 2011 CryoVEx field campaign in the pack ice north of Ellesmere Island. Also, we summarize results from another comparison of OIB with in situ snow depth data from the Bromine, Ozone and Mercury Experiment (BROMEX) (Webster and others, 2014). Both comparisons show evidence of the presence of side-lobe artifacts.

4.1. 2011 CryoVEx

Our original intent was to assess the quality of OIB ice thickness retrievals using ground measurements. However, OIB ice thicknesses are not available at this CryoVEx site, probably due to the absence of open leads needed to serve as local sea surface reference for freeboard calculations in this region of relatively compact ice. Thus our analysis is limited to the assessment of OIB snow depths. The presence of side-lobe artifacts in this comparison of OIB snow depths with CryoVEx ground surveys is indicated in the following analysis.

The surveyed line shows a large difference in mean snow depth (from ~20 to ~40 cm) between the western and eastern parts of the survey line that is bisected with a pressure ridge over 2 m high (Fig. 4d). Near the crest of the ridge, the snow depth is up to 1.5 m. The asymmetric snow distribution along the line is likely due to a vast snowdrift on the west side of the ridge.

On 15 April 2011 the OIB P-3 flew over the CryoVEx site five times. Here we examine the three tracks (a, b and c) that are closest to the snowline. The DMS imagery, ATM elevations and snow radar returns from OIB track a are shown in Figure 5a–c. The ridge (with sail height >2 m) shows up clearly in the DMS imagery and ATM elevations. The low radar returns near ridges have been noted by Kwok and others (2011) and may be due to decorrelation of radar returns over rough surfaces. The higher ATM snow surface elevations, evident on the SO (west) side of the ridge (Fig. 5d), also indicate the presence of the snowdrift/dunes with thicker snow. Visually, the snow radar echograms (Fig. 5c) also show thicker snow in the western part of the profile. However, as we show next, this was not captured by the OIB snow retrievals.

Figure 5d compares the OIB snow depths (40 m spacing) from the three tracks with those from the in situ line. It can be seen that the algorithm correctly picks some of the 30–60 cm thick snow on the eastern side of the profile. However, mean snow thicknesses are biased low by numerous low snow depths. To compare the differences between OIB and in situ measurements, we compute the difference between each ground measurement (40 m running average) and its closest OIB retrieval. The differences are -30 ± 27, -11 ± 18 and -25 ± 16 cm for tracks a, b and c, respectively, with an overall difference of -21 ± 20 cm. Even allowing for local variability in snow depth and misregistration of the corresponding measurements, these

https://doi.org/10.3189/2015JoG14J229 Published online by Cambridge University Press

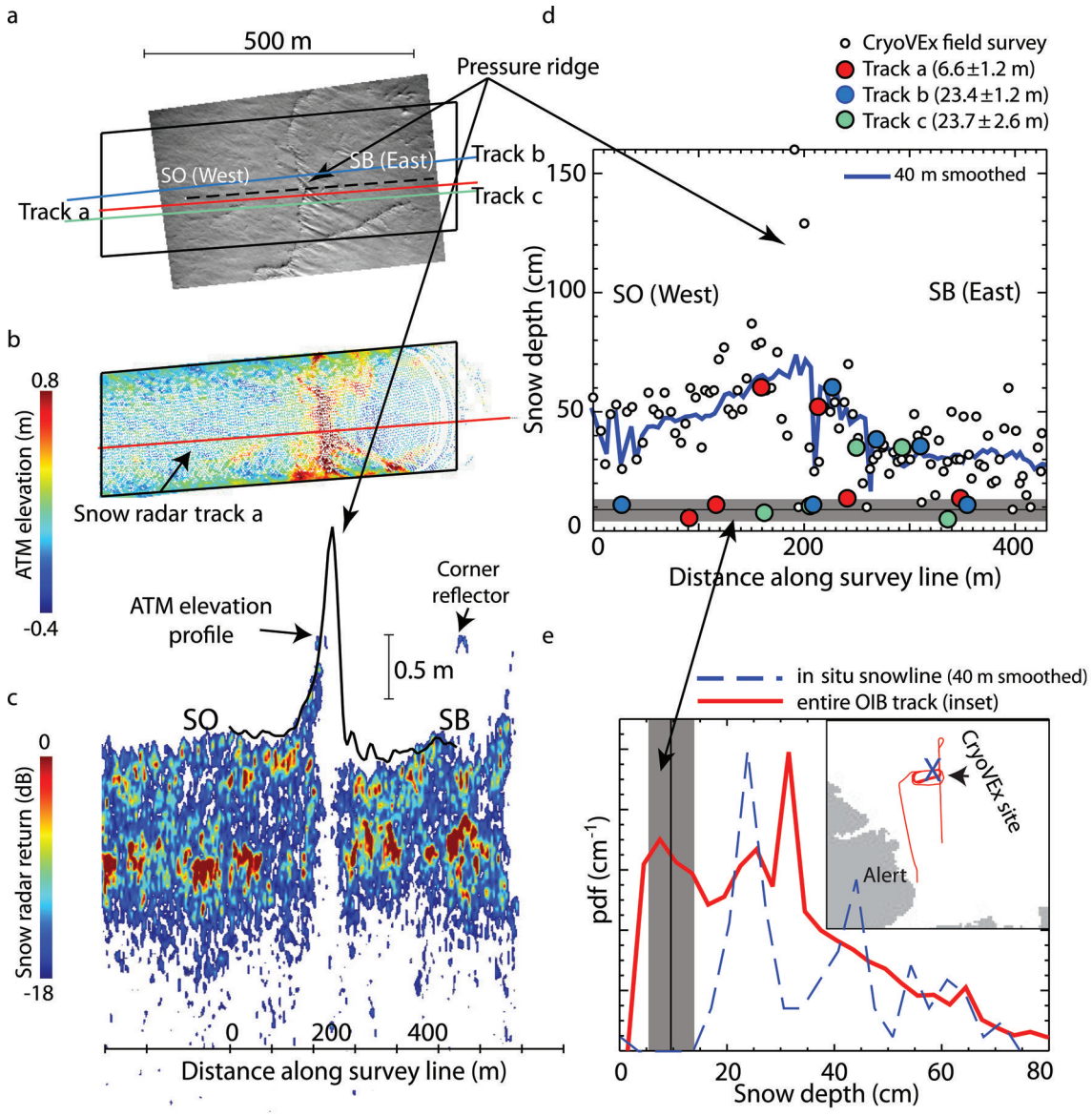

Fig. 5. Comparison of OIB snow depths with CryoVEx ground surveys in 2011. (a) Ground survey line (black dashed) and three OIB tracks (a, b, c) overlaid on camera (DMS) image of the CryoVEx south site. (b) Surface elevation from ATM lidar scans (track a). (c) Strength of radar returns (high backscatter in red) along the snow radar track a shown in (b). ATM elevation profile along track a (in black) shows pressure ridge sampled by the ground survey. (d) Snow depths from ground survey and OIB retrievals for the three tracks (a, b, c). Quantities in parentheses show average distance between each OIB retrieval and its nearest ground sample. (e) Snow depth distributions of the OIB retrievals over the inset track and along the CryoVEx snowline (40 m running average to match the OIB retrievals). Arrow between (d) and (e) shows the correspondence between OIB retrievals and the peak in the snow depth distribution histogram at ~10 cm (also visible in Fig. 4).

differences are significant. The OIB averages depict a snow cover that is on average >21 cm thinner than that of the ground survey. Closer examination of the comparisons (Fig. 5d) reveals a band of OIB retrievals at ~10 cm, with very low variability (Fig. 5d, gray band), which corresponds to the spike located at 10 cm in the snow depth distribution of the entire OIB track on 15 April (Fig. 5e, inset). Even though there are areas of shallow snow in the in situ measurements, the spike of retrieved snow depths should not cluster near the thin part of the in situ snow depth distribution. Moreover, this spike at ~10 cm is seen in all the 2011 snow depth distributions (Fig. 4b) discussed earlier, and is thus likely an artifact of the OIB retrieval procedure and product. A much smaller difference of 6 ± 17 cm was obtained after we removed snow thicknesses <15 cm from the comparison (9 of 17 points were removed). If these artifacts are ubiquitous and cannot be treated as retrieval noise then they will impact ice thickness retrievals.

It is unfortunate that OIB ice thickness estimates were not available for comparison with these CryoVEx field measurements, as underestimates of snow depth will lead to overestimates of ice thickness estimates, which will demonstrate uncertainties more clearly.

4.2. BROMEX vs OIB snow depth comparisons

In March 2012 during the BROMEX field campaign, a snow depth comparison was made between coordinated in situ and OIB measurements. Webster and others (2014) reported that the OIB snow depth product appears to underestimate thin snow depths in comparison with in situ averages. They found a clear discrepancy along one of their transects (fig. 4 in Webster and others, 2014), where the OIB quick-look and

https://doi.org/10.3189/2015JoG14J229 Published online by Cambridge University Press

standard products estimate a snow thickness of ~5–8 cm, while the in situ mean is ~23 cm. The snow depth of ~5–8 cm appears to be associated with the leading edge of the main lobe, very close to the resolution limit of the radar (Fig. 4b). Again this highlights the visible effects of the system impulse response on snow depth distributions.

5. DISCUSSION

The effects of main lobes and side lobes are present in all radar returns and are prominent characteristics of band-width-limited radar systems. In a recent analysis of snow radar data, Kwok and Maksym (2014) noted that side lobes from the stronger scattering snow–ice interfaces could be misidentified as returns from the weaker air–snow interfaces during snow depth retrieval. They also noted the need for these system effects to be considered in retrieval algorithms. Our results show spikes in the snow depth distributions that are aligned with the location of system main- and side-lobes, and thus are sources of errors if these products are used in geophysical analysis. These artifacts affect the accuracy of the snow depth product and suggest that geophysical results from earlier studies utilizing these products may need to be re-examined. Here we summarize our findings and discuss the need for an improved approach for snow depth retrieval.

First, the current OIB algorithm (Kurtz and others, 2013) uses the local maxima as well as leading edge to locate the air–snow interface, which implies that the retrieval procedure is likely sensitive to system main- and side-lobes in the radar returns. Such an approach creates systematic errors when identifying the location of the air–snow interfaces in OIB products. However, quantitative assessment of the effects of these side lobes on overall snow depth statistics in the present OIB products is difficult. Removal of the population under the spikes makes the resulting mean snow depths smaller or larger, as the results depend on the location of the spikes and the overall regional snow depth distributions. Moreover, removal of biased data in the distribution, by creating gaps, does not address the resultant omission errors in sampling. A more comprehensive retrieval approach that addresses these artifacts is needed.

Second, the effects of the side lobes are also evident when the OIB retrievals are compared with in situ snow depth measurements from a CryoVEx ground survey in 2011. In the case considered here, retrieval OIB snow depths contaminated by side-lobe artifacts depicts a snow cover that is on average >20 cm thinner than that of the ground survey. Discrepancies between OIB snow depth products and in situ measurements from BROMEX have also been reported (Webster and others, 2014).

Third, since the locations and strength of side lobes vary with each radar installation, their impact needs to be addressed for each campaign. For example, for snow depth over MY ice at the end of winter, the distributions with the spikes due to side lobes below 25 cm in 2011 and 2012 would lead to underestimates of mean retrieved snow depths although with different effects. It is clear that the issue of side lobes should be addressed explicitly in the design of improved retrieval procedures either by suppressing them in the processing of the radar signals (i.e. deconvolution of the expected response) or by addressing the issue in the detection scheme (e.g. Kwok and Maksym, 2014; Newman and others, 2014).

The ramifications of the three points expressed above impact estimates of sea-ice thickness from ice freeboard. Since ice freeboard is obtained by subtracting OIB snow depth estimates from measured snow freeboard, the impact of OIB snow depth estimates that are too thin is clear: biases introduced into thickness estimates could be many times the biases in the snow depth retrievals.

6. CONCLUSIONS

In our examination of four years (2009–12) of published OIB Level 2 products of Arctic snow depth, we found retrieval artifacts that stem from side lobes and main lobes in the radar returns. This highlights the need for consideration of the impulse response of the radar in the design of improved snow depth retrieval algorithms. Recent authors have addressed some of these issues by introducing new processing approaches (e.g. Kwok and Maksym, 2014; Newman and others, 2014), but an improved approach for routine processing of the radar data remains to be devised. At present, there is a community effort to identify the best possible algorithms for mitigation of these effects: a Snow Thickness On Sea Ice Working Group (STOSIWIG) has been formed by NASA to address the system and geophysical issues associated with snow depth retrieval.

ACKNOWLEDGEMENTS

We thank Shirley Pang for software support during the course of this study. Data from OIB are provided by the NSIDC. CryoVEx data are available through the ESA data portal: http://earth.esa.int. R.K. performed this work at the Jet Propulsion Laboratory, California Institute of Technology, under contract with NASA.

REFERENCES

Brucker L and Markus T (2013) Arctic-scale assessment of satellite passive microwave-derived snow depth on sea ice using Operation IceBridge airborne data. *J. Geophys. Res.*, **118**(6), 2892–2905 (doi: 10.1002/jgrc.20228)

Farrell SL and 9 others (2012) A first assessment of IceBridge snow and ice thickness data over Arctic sea ice. *IEEE Trans. Geosci. Remote Sens.*, **50**(6), 2098–2111, (doi: 10.1109/tgrs.2011.2170843)

Koenig L, Martin S, Studinger M and Sonntag J (2010) Polar airborne observations fill gap in satellite data. *Eos*, **91**(38) (doi: 10.1029/2010eo380002)

Krabill WB (2013) *IceBridge ATM L1B elevation and return strength, Version 2*. NASA Distributed Active Archive Center, National Snow and Ice Data Center, Boulder, CO http://nsidc.org/data/i/ilatm1b

Krabill WB and 8 others (2002) Aircraft laser altimetry measurement of elevation changes of the Greenland ice sheet: technique and accuracy assessment. *J. Geodyn.*, **34**, 357–376

Kurtz NT and Farrell SL (2011) Large-scale surveys of snow depth on Arctic sea ice from Operation IceBridge. *Geophys. Res. Lett.*, **38**(20), L20505 (doi: 10.1029/2011gl049216)

Kurtz NT, Studinger MS, Harbeck J, Onana V and Farrell S (2012) *IceBridge sea ice freeboard, snow depth, and thickness*. NASA Distributed Active Archive Center, National Snow and Ice Data Center, Boulder, CO http://nsidc.org/data/idcsi2.html

Kurtz NT and 8 others (2013) Sea ice thickness, freeboard, and snow depth products from Operation IceBridge airborne data. *Cryosphere*, **7**, 1035–1056 (doi: 10.5194/tc-7-1035-2013)

Kwok R and Maksym T (2014), Snow depth of the Weddell and Bellingshausen Sea ice covers from IceBridge surveys in 2010

https://doi.org/10.3189/2015JoG14J229 Published online by Cambridge University Press

and 2011: an examination. *J. Geophys. Res.*, **119**(7), 4141–4167 (doi: 10.1002/2014JC009943)
Kwok R and 6 others (2011) Airborne surveys of snow depth over Arctic sea ice. *J. Geophys. Res.*, **116**(C11), C11018, (doi: 10.1029/2011JC00737)
Laxon SW and 14 others (2013) Cryosat-2 estimates of Arctic sea ice thickness and volume. *Geophys Res. Lett.*, **40**(4), 732–737 (doi: 10.1002/grl.50193)
Leuschen C (2010) *IceBridge snow radar L1B geolocated radar echo strength profiles*. NASA Distributed Active Archive Center, National Snow and Ice Data Center, Boulder, CO http://nsidc.org/data/irsno1b/versions/1
Lindsay R and 9 others. (2012), Seasonal forecasts of Arctic sea ice initialized with observations of ice thickness. *Geophys. Res. Lett.*, **39**(21), L21502 (doi: 10.1029/2012gl053576)
Martin CF and 6 others (2012) Airborne topographic mapper calibration procedures and accuracy assessment. *NASA Tech. Rep.* Vol. 20120008479 (NASA/TM-2012-215891, GSFC. TM.5893.2012)
Newman T and 6 others (2014) Assessment of radar-derived snow depth over Arctic sea ice. *J. Geophys. Res.*, **119**(12), 8578–8602 (doi: 10.1002/2014JC010284)
Panzer B and 8 others (2013) An ultra-wideband, microwave radar for measuring snow thickness on sea ice and mapping near-surface internal layers in polar firn. *J. Glaciol.*, **59**(214), 244–254 (doi: 10.3189/2013JoG12J128)
Richter-Menge JA and Farrell SL (2013) Arctic sea ice conditions in spring 2009–2013 prior to melt. *Geophys. Res. Lett.*, **40**(22), GL058011 (doi: 10.1002/2013GL058011)
Webster MA and 6 others (2014) Interdecadal changes in snow depth on Arctic sea ice. *J. Geophys. Res. Oceans*, **119**(8), 5395–5406 (doi: 10.1002/2014JC009985)
Willat RS and Haas C (2011) CryoVEx 2011 Alert sea ice ground team report. Internal European Space Agency document

MS received 8 December 2014 and accepted in revised form 17 April 2015